Rev. Roum. Sci. Techn.– Électrotechn. et Énerg.
Vol. 64, 4, pp. 383–390, Bucarest, 2019

PERFORMANCE OF A SiC MOSFET BASED ISOLATED DUAL ACTIVE BRIDGE DC-DC CONVERTER FOR ELECTRO-MOBILITY APPLICATIONS

VEERA VENKATA SUBRAHMANYA KUMAR BHAJANA[1,2], WOJCIECH JARZYNA[2], KAROL FATYGA[2], DARIUSZ ZIELINSKI[2], LUKASZ KWAŚNY[2]

Key words: Dual active bridge (DAB) converter, Isolated dc-dc converter, SiC MOSFET, Phase-shift control, Zero voltage switching (ZVS)

This article describes the design and testing of a 400 V - 8 kW - 100 kHz isolated dual active bridge (DAB) dc-dc converter using four 1200 V/40 A SiC MOSFET modules. The converter is operated under hard-switching conditions by using single phase shift (SPS), extended phase shift (EPS) and dual phase shift (DPS) controls. The phase-shift angles between two DABs are optimized in order to achieve the minimized circulating current by the transformer. By varying the phase-shift angles of secondary side switching devices, the overall performance of dual active bridge dc-dc converter is analyzed. The conversion efficiencies are measured between dc input and output terminals of DAB for conventional and phase-shift PWM controls. The different operating modes and design system parameters are illustrated. The efficiency of the converter is validated by experimental results on 8 kW laboratory prototype.

1. INTRODUCTION

Nowadays, various dc-dc converters such as boost, buck, buck-boost play vital role in battery charging applications in hybrid electric vehicles. Electro-mobility is a part in battery charging stations, where, buck/boost dc-dc converters [1–3] are used to get ultrafast charging of battery. A 53.2 V, 2 kW battery based isolated bidirectional dc-dc (BDC) converter [1] has been developed to obtain 305 V output voltage operated at 6 kW output power and achieved 96 % efficiency. However, this converter is operated at switching frequency of 20 kHz. A phase-shift control [2–4] is introduced to minimize the dc offsets through the transformer currents, which results in reduced peak currents by the switching devices. Furthermore, commutation inductance is serially connected with primary side transformer of dual active bridge (DAB) [5, 6], and its performance is analyzed by two different zero voltage switching methods namely current-based and energy based (CB-ZVS) methods. A 350 V / 10 kW isolated bidirectional converter [7] performance has been evaluated by trench gate insulated gate bipolar transistors (IGBTs) as switching devices with overall efficiency of about 97 %. However, it is operated under very low switching frequency. The impact of loss-less snubber capacitor and dead-time influence on dc-dc converters [8, 9] was presented for proper charging and discharging of the input capacitor bank. In order to reduce the surge currents of the transformer and to keep a stable maximum power transfer, a hybrid dual phase shift control has been used for bidirectional converters [10, 11] based on IGBT switching devices. Moreover, researchers have investigated the soft-switching isolated dc-dc [12], bidirectional converters with additional series resonant elements [13–16]. However, in the present days, the design and usage of efficient SiC MOSFETs modules in dc-dc converters [17, 18] is increased for battery charging applications. This paper presents an isolated dc-dc converter's design using four modules of SiC MOSFET and its performance has been analyzed under two different operating conditions.

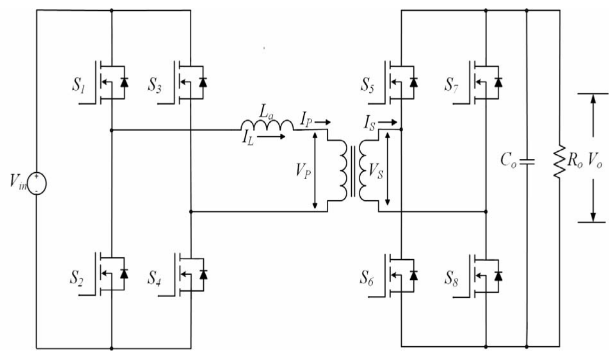

Fig. 1 – SiC MOSFET based dual active bridge (DAB) dc-dc converter.

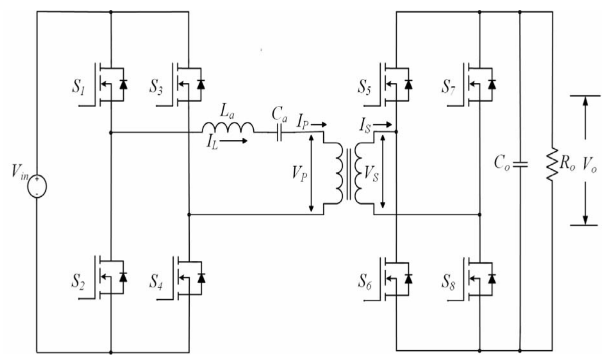

Fig. 2 – SiC MOSFET dual active bridge (DAB) dc-dc converter with series resonant network.

This dual active bridge (DAB) dc-dc converter is operated at 400 V input voltage and has a maximum output power of 8 kW. Two operating conditions are used in this converter that, one is the series connection of commutation inductance with primary side of transformer and the other is the connection of series resonant elements. Both the performances were evaluated under the open loop circumstances. In this paper, the operating stages of converter and design guidelines are elucidated in the following Section 2. The experimental results and

[1] School of Electronics Engineering,KIIT University, Bhubaneswar-751024,Odisha, India, E-mails: kumarbvvs@yahoo.co.in, bvvs.kumarfet@kiit.ac.in.
[2] Faculty of Electrical Engineering and Computer Science, Department of Electrical Drives and Machines, Lublin University of Technology, 20 – 618 Lublin, Poland.

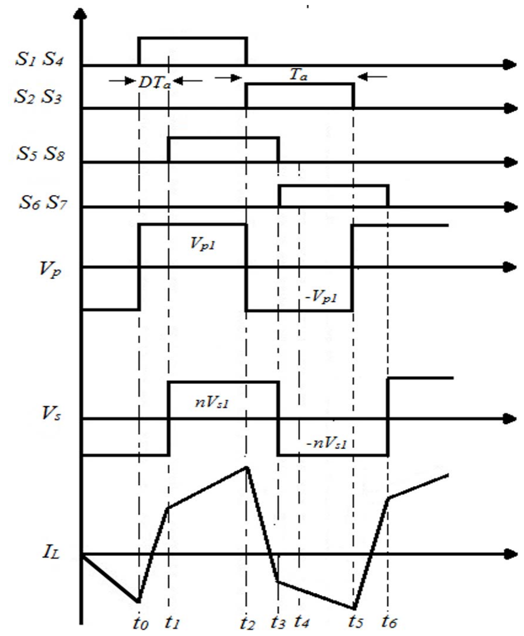

Fig. 3 – Single phase shift control key waveforms.

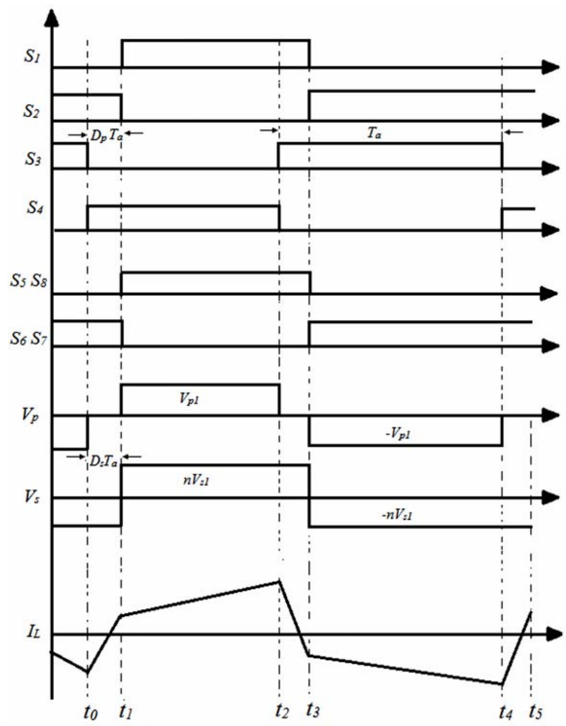

Fig. 4 – Extended phase shift control key waveforms.

efficiency comparisons are presented in Sections 3 and 4, respectively.

2. DESCRIPTION OF THE DUAL ACTIVE BRIDGE (DAB) CONVERTER AND ITS OPERATION PRINCIPLES

The principle of operations are described for the single phase shift (SPS), extended phase shift (EPS) and dual phas shift (DPS) pulse width modulation (PWM) controlling techniques. Figure 1 shows the SiC MOSFET based DAB dc-dc converter with a series inductor and Fig. 2 illustrates that SiC MOFET based DAB converter with series resonant network, respectively.

2.1 SINGLE PHASE SHIFT CONTROL OPERATION

The key waveform shown in Fig. 3 represents the voltage and currents of the transfomer. The main circuit comprises of S_1,S_2,S_3,S_4 for primary side and S_5,S_6,S_7,S_8 for secondary side. In addition, an auxiliary inductor L_a and high frequency transformer are used to transfer the energy to load. The two diagonal switches S_1,S_4 are turned-on at the same time and S_2,S_3 turns on as complimentary fashion to that S_1,S_4 with 50 % duty cycle (D), which is shown in Fig. 3. Secondary side switching devices S_5,S_8 and S_6,S_7 are turned on same as the primary switches. The primary and secondary side bridges are operated with 50 % duty ratios with a phase shift angle (ϕ) during the interval t_0–t_1 and is equal to DT_a where $D = \phi / \pi$, as it is represented in Fig. 3. The gate control signals, S_1–S_4 corresponding to primary bridge switches and secondary bridge control signals, S_5–S_8 are shown in Fig. 3. The primary and secondary voltages are denoted as V_P and V_S, respectively. The change in direction of current, I_L (I_L= $i_{La}(t)$) takes place during the phase shifts of the intervals t_0–t_1 and t_2–t_3. The operation during the intervals from t_0-t_4 are divded into four modes, in which S_1, S_4 and S_5, S_8 from primary and secondary switches, respectively, are operated with a phase angle DT_a. During the interval, t_4–t_6, the switches S_2, S_3 and S_6, S_7 are operated with a phase shift and the operation is same as that of interval, t_0–t_2, except for the direction of current, I_L.

Mode 1: During this mode at time t_0, the switches S_1,S_4 are turned-on, the V_{in} is applied at primary side and output voltage is clamped at secondary side by switching S_6,S_7. The energy stored by the inductance L_a prior to this mode, flows through the primary side with decreasing primary current at a slope (rate of change of current), that is expressed in (1).

$$i_{La}(t) = i(t_0) + \frac{V_{p1} - (nV_{s1})}{L_a}(t - t_1) \, , \tag{1}$$

where $n = n_1/n_2$ are primary and secondary turns ratio, V_{p1} is input voltage, V_{s1} is the output voltage and L_a is auxiliary inductor.

Mode 2: During this mode from t_1–t_2, the switches S_1,S_4 and S_6,S_7 are in conducting state same as the previous mode. The occurance of a positive magnitude of primary current is only the difference from the first stage, which represents the inductance L_a by charging up.

Mode 3: At t_2, the secondary side switches S_5,S_8 are turned on and S_1,S_4 are still in conducting state. The energy stored in auxiliary inductor L_a is delivered as output by a large filter capacitance.

Mode 4: At t_3, the switches S_1,S_4 are turned-off and the switches S_2,S_3 are turned-on. There is a decreasing magnitude of primary current which shows that the energy stored by auxiliary inductor L_a flows towards the input. The current slope of the primary side is defined as

$$i_{La}(t) = i(t_3) - \frac{(nV_{s1})}{L_a}(t - t_4) \, . \tag{2}$$

2.2 EXTENDED PHASE SHIFT CONTROL

Figure 4 shows the idealized waveforms of voltage and currents of primary side and secondary side of the converter. To reduce the backward flow of power transfer by using SPS control, the primary side switches with an inner phase shifts have been introduced in EPS control. However, the two full bridges are operated with a phase shift. The diagonal switches of primary side, S_1,S_4 and S_2,S_3 are turned on with a inner phase shift to decrease the energy transfer by auxiliary inductance to the source. The energy transfer to source by an auxiliary inductor L_a becomes zero, because the transformer primary voltage is zero for the time interval t_0–t_1 and t_2–t_3. Therefore, the power transfer to source is decreased in an overall power transfer. In this EPS control, the phase shift introduced between the diagonal switching devices is denoted as D_pT_a in Fig. 4. As it can be seen from Fig. 4, the transformer primary voltage is quasi square wave and secondary voltage remains square wave. By introducing inner phase shift between diagonal switches, primary side voltage results in quasi square wave *i.e.* three level voltage, which is different from the two level (*i.e.* SPS control). Consequently, extended phase shift controls by inner phase shift operation decreases the current stresses and extend the power transfer capability. The operation of EPS divided into seven intervals t_0–t_7. As it can be seen from Fig. 4, change of direction of current I_L ($I_L = i_{La}(t)$) during the intervals t_0–t_1 and t_2–t_3.

Interval t_0–t_1: Prior to time t_0, the switches S_2,S_3 are conducting. At time t_0, the switch S_3 is turned-off and S_4 is turned-on. During this interval, the current of the auxiliary inductor L_a is negative, hence, the L_a current is carried to input source. Secondary side switches S_6,S_7 are turned-on to transfer the load current by L_a. At the end of t_1, the current of L_a reached zero. The current I_L (($I_L = i_{La}(t)$) is expressed as follows

$$i_{La}(t) = i_{La}(t_0) + \left(\frac{V_{p1} + nV_{s1}}{L_a}\right)(t - t_1)\,. \tag{3}$$

Interval t_1–t_2: Beginning of this interval at t_1, the switch S_1 is turned-on and L_a current is in positive direction and secondary side current is carried to output load by means of S_5,S_8 switches. The voltage across L_a is clamped to V_{p1} + nV_{s1}. At the end of t_2, S_4 is turned-off. The current I_L ((I_L= $i_{La}(t)$) is expressed as

$$i_{La}(t) = i_{La}(t_1) + \left(\frac{V_{p1} - nV_{s1}}{L_a}\right)(t - t_2)\,. \tag{4}$$

Interval t_2–t_3: At time t_2, the switch S_3 is turned-on, the current of L_a starts decreasing linearly towards zero and voltage of the primary side becomes zero throughout this interval. Hence, there is an energy flows through the input source by the L_a. At the end of this interval, S_1 is turned-off and S_2 is turned-on at t_3 and secondary side switches S_6,S_7 are turned-on. The current I_L ((I_L= $i_{La}(t)$) is expressed as

$$i_{La}(t) = i_{La}(t_2) + \left(\frac{-nV_{s1}}{L_a}\right)(t - t_3)\,. \tag{5}$$

Interval t_3–t_4: From the beginning of this interval, the switches S_2,S_3 and S_6,S_7 are turned-on and output power is transferred to the load. The current of L_a (I_L= $i_{La}(t)$) flows in negative direction.

The time interval t_4–t_5 is same as the t_0–t_1 interval.

2.3 DUAL PHASE SHIFT CONTROL:

In single phase shift (SPS) control, there is a single phase shift between two primary and secondary bridges and with extended phase shift, there is an inner phase shift between the two half bridges at primary side only. In order to reduce the reactive power and current flows through the source, the other control dual phase shift control (DPS) is used. In DPS there are phase shifts in primary side and also secondary side switches as well. Figure 5 shows the primary voltage $V_{p1,}$ secondary voltage V_{S1}, I_L is primary current (I_L= $i_{La}(t)$) through L, the transformer voltage ratio, n and gating control signals S_1–S_8. In this DPS control, inner phase shift (D_pT_a) and outer phase shift (D_sT_a), corresponds to primary and secondary, respectively. Whereas phase shift between the legs of primary is inner and phase shift between dual bridges represents as outer. Both primary and secondary voltages are quasi square wave, since both bridges are operating with a phase shift. In DAB converters, the DPS control offers high output power in comparison with the SPS, EPS control techniques.

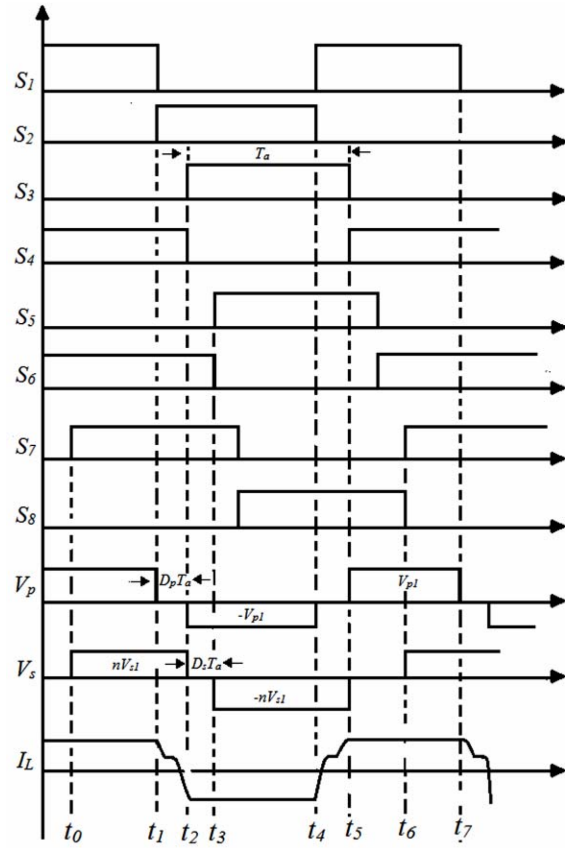

Fig. 5 – Dual phase shift control key waveforms.

The direction of the primary current, I_L changes during the intervals t_1–t_2 and t_4–t_5. It can be seen that the peak currents of the primary are much smaller than those of SPS control. The operation of DPS control is divided into seven intervals t_0–$t_{7,}$ are discussed as follows:

Interval (t_0–t_1): From the beginning of this interval, the switches S_1,S_4 are conducting and the current of the L_a flows via secondary side by S_6,S_8 which are already being conduction. The current I_L ((I_L = $i_{La}(t)$) is expressed as follows

$$i_{La}(t) = i_{La}(t_0) + \left(\frac{V_{p1} - nV_{s1}}{L_a}\right)(t - t_1)\,. \tag{6}$$

Interval (t_1–t_2): At time t_1, the S_1 is turned off, S_2 is turned-on and S_4 still conducts. The L_a current linearly decreasing to zero and then becomes zero. At the end of this interval, the S_4 is turned-off. The current slope of the primary side is defined as

$$i_{La}(t) = i_{La}(t_1) + \left(\frac{-nV_{s1}}{L_a}\right)(t - t_2)\,. \quad (7)$$

Interval (t_2–t_3): At t_2, the switch S_3 is turned-on and its diagonal switch S_2 is already turned-on in previous interval. The L_a current direction is changed from positive to negative and it transferred to load by turning on S_5 at t_2, and S_7 is still conducting. At the end of this interval t_3, the switch S_7 is turned-off and S_8 is turned-on.

Interval (t_3–t_4): The switches of primary side S_2,S_3 and secondary side S_5,S_8 are conducting to transfer the power throughout this interval. At time t_4, the switch S_3 is turned-off and the L_a current reaches zero. The current I_L is expressed as follows

$$i_{La}(t) = i_{La}(t_3) + \left(\frac{-nV_{p1}}{L_a}\right)(t - t_4)\,. \quad (8)$$

Interval (t_5–t_6) is same as the first interval (t_0-t_1).

2.4 ZERO VOLTAGE SWITCHING OPERATION

In addition to hard-switching, a soft-switching operation is also presented in this section. The main intention of this paper is to evaluate the dual active bridge (DAB) converter performance in two cases, one is hard-switching condition and another is soft-switching condition respectively. The conventional DAB converter with a series additional inductance L_a at primary side bridge is shown in Fig. 1. Whereas, the analysis for three different controls have been discussed in this section. The extended phase shift minimizes the energy back to the input side during the interval t_0–t_1 of SPS. However, the back energy affects the overall efficiency of DAB converter. In order to improve the voltage conversion ratio, overall efficiency and minimal current stress in those two controls, the theoretical analysis is given on series resonant DAB converter as shown in Fig. 2. The corresponding idealized voltage and currents of the primary side of transformer is shown in Fig. 6. In the operation of the DAB converter while it is in single phase shift control, there is a back energy transfer to input source is suppressed during the interval t_0–t_1 shown in Fig. 6, which shows that the body diode of corresponding switches gives path for resonant tank current. The soft-switching turn-on operation (zero voltage switching) is achieved for all switching devices throughout the operation. This resonating operation results the continuous current flow across transformer. Similarly, Fig. 7 shows the idealized voltage and current waveforms of DAB converter when it is operated under dual phase shift control. During the interval t_0–t_1, the current of resonant tank starts from zero (soft-turn-on operation is observed, *i.e.*, it conducts without body-diode), the current of the switches smoothly increasing from zero and decreasing to zero.

3. **ANALYSIS OF SPS, EPS, DPS**

When the converter is operating with single phase shift control (SPS), the current stresses of the switching devices is increased depends on total amount of time energy transfer to input source. The average current of the L_a is obtained by solving (1) to (2). Current stress of the converter $i(t_0)$ for the interval (t_0–t_1) is defined by (9).

$$i(t_0) = \frac{nV_{p1}V_{s1}}{4f_sL_a}\left[2D - 1 + k\right]. \quad (9)$$

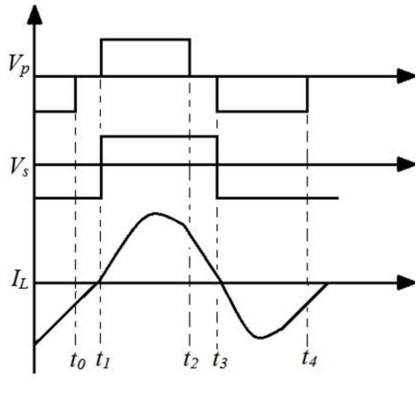

Fig. 6 – EPS soft-switched.

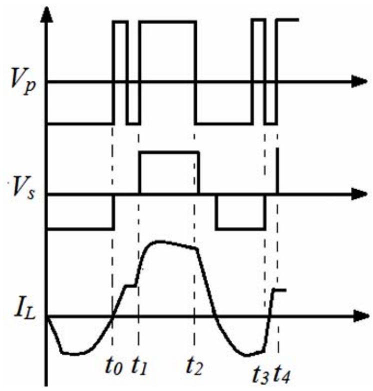

Fig. 7 – DPS soft-switched.

Here, switching frequency $f_s = \dfrac{1}{2T_p}$, voltage conversion ratio $k = \dfrac{V_{in}}{nV_o}$. When $k < 1$, the power transfers from V_{in} to V_o.

While the converter is operating under conventional phase shift control, the transmitted power (P) is expressed as equation (10).

$$P = \frac{nV_{p1}V_{s1}}{2f_sL_a}\left[D(1-D)\right]. \quad (10)$$

In order to minimize the energy transfer to the source during the interval t_0–t_1 (Fig. 4), an extended phase shift (EPS) control is used, which will reduce the flow of energy by L_a to the input source. When extended phase shift control (EPS) is used, the current stresses of switching devices is minimized and it is expressed in equation (6) by solving the equations (3),(4),(5).

$$i(t_0) = \frac{nV_{p1}V_{s1}}{4f_sL_a}\left[k(1-D_p) + (2D_p + 2D_s - 1)\right], \quad (11)$$

where $$k \le \frac{1-2D_s}{1-D_p}. \quad (12)$$

The energy transfer to the source occurs during the interval (t_0–t_1) if the parameter $k < 1$ and $D_S + D_p \le 1$. Otherwise, there is no power flow to the source, where D_s is duty cycle of secondary bridge, D_p is duty cycle of primary bridge.

$$P = \frac{1}{T_a}\int_0^{T_a} V_p i_L(t)\mathrm{d}t.$$

$$P=\frac{nV_{p1}V_{s1}}{2f_sL_a}\left[D_s(1-D_s)+\frac{1}{2}D_p(1-D_p-2D_s)\right]. \quad (13)$$

$$i(t_0)=\frac{(-1+D_p)V_{p1}+(1+D_p-2D_s)nV_{s1}}{4f_sL_a}. \quad (14)$$

$$P=\frac{nV_{p1}V_{s1}(-2D_p+D^2p-(-2+D_s)D_s)}{4f_sL_a}. \quad (15)$$

The soft-switching conditions for the switching devices are obtained by means of connecting the series resonant elements at primary side. The voltage through the primary side $V_p(t)$ is expressed as in equation (16) and current of the primary side $i_p(t)$ is defined as in equation (17). The output power is defined by equation (18) and the equivalent impedance Z_p is defined by equation (19), respectively.

$$V_p(t)=\frac{4nV_o}{\pi}\sin\omega t. \quad (16)$$

$$i_p(t)=A\sin(\omega t-\varphi). \quad (17)$$

$$P_o=\frac{2\sqrt{2}nV_o}{\pi}\frac{A}{\sqrt{2}}\cos\varphi=\frac{V_o^2}{R_o}, \quad (18)$$

where $A=\dfrac{\pi V_o}{2nR_o\cos\varphi}$; A is amplitude of $i_p(t)$.

$$Z_p=\overline{V_p(t)}\Big/\overline{i_p(t)}=\frac{8n^2R_o\cos\varphi}{\pi^2}\angle\varphi. \quad (19)$$

The voltage gain of the DAB converter is defined in (20) and its simplified equation is (21)

$$G=\left|\frac{Z_p\text{II}\mathrm{j}\omega L_m}{Z_p\text{II}\mathrm{j}\omega L_m+\mathrm{j}\omega L_a+\dfrac{1}{\mathrm{j}\omega C_a}}\right|, \quad (20)$$

$$G=\frac{1}{\sqrt{\left[1+\dfrac{1}{k}\left(1-\dfrac{1}{x^2}\right)\right]^2+Q^2\left(x-\dfrac{1}{x}\right)^2}}, \quad (21)$$

where $k=\dfrac{L_m}{L_a}$; $Q=\dfrac{\pi^2Z}{8n^2R_o}$; $y=\dfrac{f_s}{f_r}$;

$$f_r=\frac{1}{2\pi\sqrt{L_aC_a}}. \quad (22)$$

3.1 DESIGN EXAMPLE

The DAB converter resonating elements are designed for the following considerations: V_{in} = 400 V, V_o = 260 V, switching frequency of 100 kHz, output power P_o = 8 kW.

The normalized frequency *y* should be less than or equals to 1 in order to keep resonant frequency f_r below the operating switching frequency f_s, whereas switching frequency is 100 kHz and resonant frequency is about 91 kHz. The impedance of the resonant network would be 8.6 ohms. The parameter *k* should be below 6, the magnetizing inductance 100 µH and auxiliary inductor L_a is 15 µH are chosen respectively. The resonant frequency should be below the switching frequency in order to obtain soft-switching. The values of resonant inductance L_a is 15 µH and resonant capacitance C_a is 200 nF have been chosen to keep resonant frequency at 90 kHz. The *Q* value was chosen below 0.5 and the overall gain (*G*) is 1.066, which is calculated by equation (20).

4. EXPERIMENTAL RESULTS

In this paper, the performance evaluation of dual active full-bridge dc-dc converter has been presented. The experimental results were measured by using four SiC MOSFET modules. Furthermore, the efficiency analysis was performed by single phase shift, extended phase shift and dual phase shift control techniques as well. A 400 V / 8 kW converter system operated under 100 kHz switching frequency is used in this converter. The converter system parameters considered are mentioned in Table 1. Firstly, this converter system was tested under phase shift angle 11° (*i.e.*, equals to 0.33 µs), which is basically traditional phase shift control between primary and secondary full bridges.

Table 1

Components and parameters: experimental

Parameters	Symbol	Value
Input voltage	V_{in}	400 V
Output voltage	V_o	260 V
Output power	P_O	8 kW
Switching frequency	f_{SW}	100 kHz
Resonant capacitor	C_a	200 nF
Resonant inductor (Ferrite Core E-70)	L_a	15 µH
Magnetizing inductance	L_m	100 µH
SiC MOSFETs	(S_1–S_4)	FF11MR12W1M1_B11
High frequency transformer	HFT	FERYSTER 5692K912
Transformer turns ratio	n	0.65
Output capacitor	(C_O)	470 µF

Figure 8 illustrates that the voltage and currents of primary and secondary sides of the transformer. The maximum efficiency obtained was 93.5 % at 8 kW output power. Then, this converter was tested with an extended phase shift control *i.e.*, there is inner phase shift beween primary side diagonal switches S_1,S_4 and S_2,S_3. The efficiency of the converter is measured by using the two different inner phase shifts angles 36° (1 µs) and 72° (2 µs). The experimental results were measured for different input voltage levels with a constant load resistance, Fig. 9 shows the obtained results at 150 V input voltage and 110 V output voltage for 36° phase shift angle.

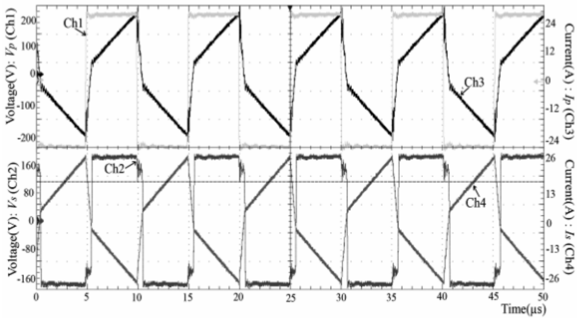

Fig. 8 –Voltage waveforms of primary and secondary side of the transformer (Ch1 : 100 V/div , Ch2: 80 V/div) and Current across the transformer primary (I_p) and secondary (I_s) (Ch3: 12 A/div Ch4 : 13 A/div) : DAB operated under hard switched : SPS control.

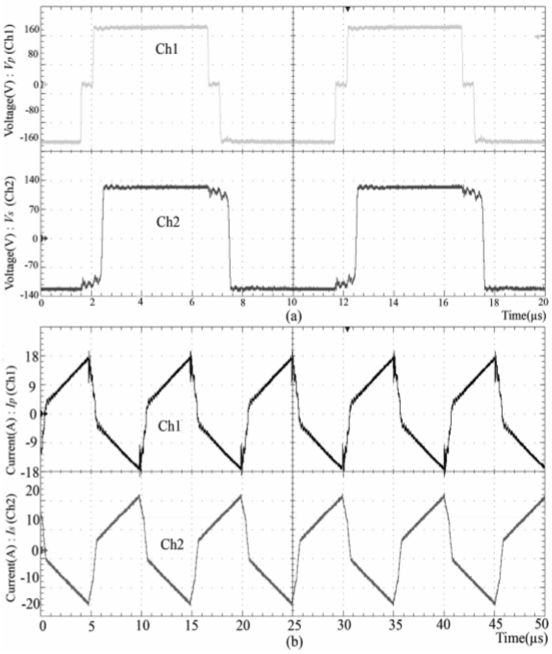

Fig. 9 – (a) Voltage waveforms of primary and secondary side of the transformer (Ch1 : 80 V/div , Ch2: 70 V/div) (b) Current across the transformer primary (I_p) and secondary (I_s) (Ch1: 9 A/div Ch2 : 10 A/div) : DAB operated under hard switched : EPS control.

Figure 10 shows the voltage through the primary and secondary side of the transformer.It is observed from the analysis that, the efficiency of the converter is increased by decreasing the phase shift angle. The efficiencies are obtained as 94.7 % and 95.5 % for 90° and 45° phase shift angles, respectively. While DAB converter is operating under EPS control, the performance analysis also made by connecting series resonant network to primary side of the transformer. Figure 11 illustrates the voltage and current waveforms of primary and secondary of the transformer, which is measured under 350 V input voltage and 250 V as obtained output voltage at 6 kW output power.

In order to improve the efficiency and reduce the current stress, this DAB converter was controlled by means of dual phase shift. So, primary side and secondary side switching devices are gated by means of inner phase shift (D_p) and outer phase shift (D_s) respectively.

While converter operating in DPS control, the phase shift angles are same for D_p and D_s . The phase shift angles for both sides are 144° (which equals to 4 μs). Figure 12 shows the measured voltage waveforms through the primary and secondary sides of the transformer for 300 V as input voltage and 260 V output voltages at 7.5 kW output power, respectively.

From these experimental analysis, it is observed that, while DAB converter operating at lower input voltage levels, the current waveform of L_a is same as ideal waveforms as shown in Fig. 5. However, when converter is operated at higher input voltage, the current waveform is

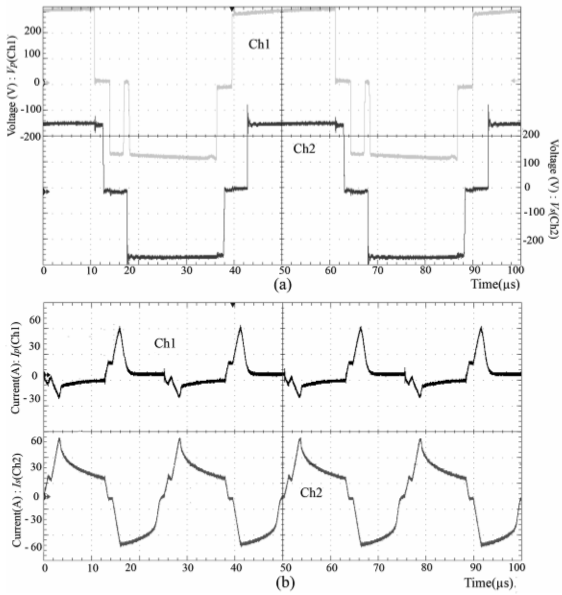

Fig. 11 – (a) Voltage waveforms of primary and secondary side of the transformer (Ch1 : 100 V/div , Ch2: 100 V/div) (b) Current across the transformer primary (I_p) and secondary (I_s) (Ch1: 30 A/div Ch2 : 30 A/div) : DAB hard switched : DPS control.

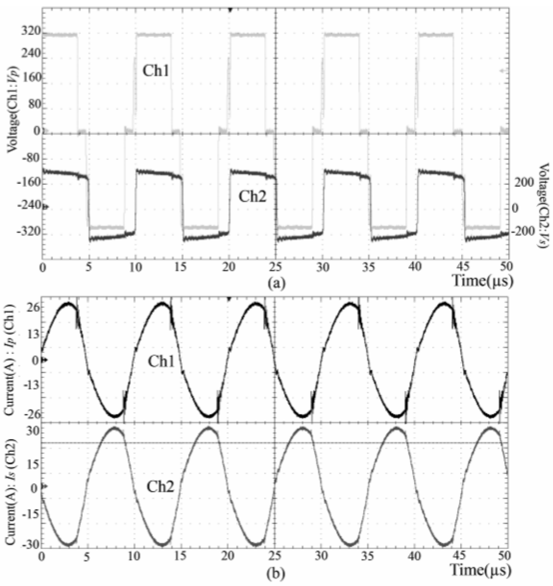

Fig. 10 – (a) Voltage waveforms of primary and secondary side of the transformer (Ch1 : 80 V/div , Ch2: 200 V/div) (b) Current across the transformer primary (I_p) and secondary (I_s) (Ch1: 13 A/div Ch2 : 15 A/div) : DAB with series resonant : EPS control.

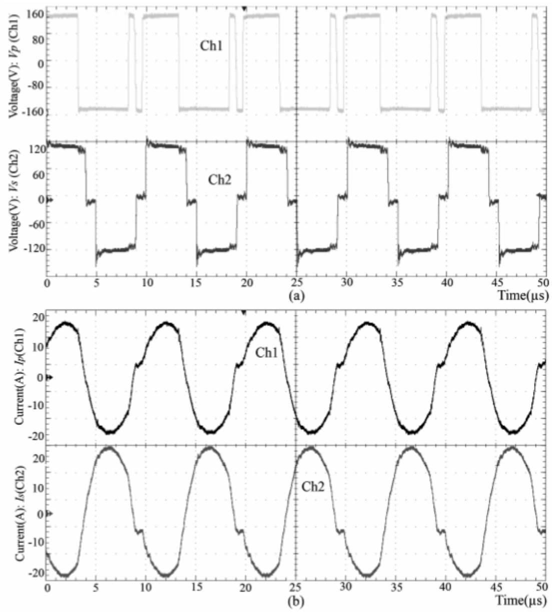

Fig. 12 – (a) Voltage waveforms of primary and secondary side of the transformer (Ch1 : 80 V/div , Ch2: 60 V/div) (b) Current across the transformer primary (I_p) and secondary (I_s) (Ch1: 10 A/div Ch2 : 10 A/div) : DAB Soft-switched : DPS control.

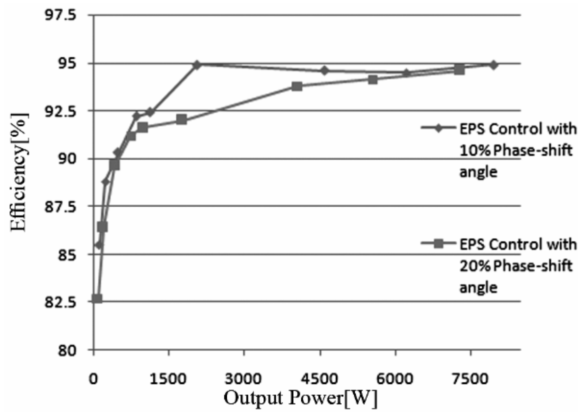

Fig. 13 –Efficiency comparisons of EPS control : hard-switching.

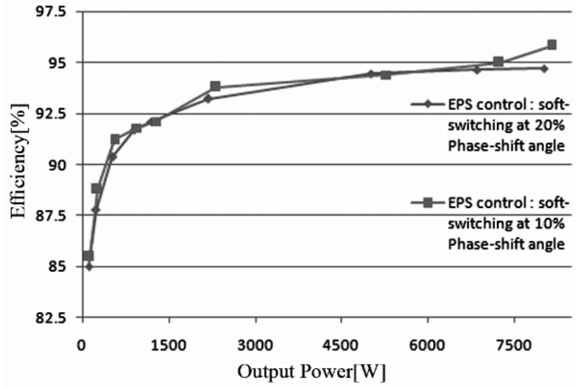

Fig. 14 –Efficiency comparisons of EPS control : soft-switching.

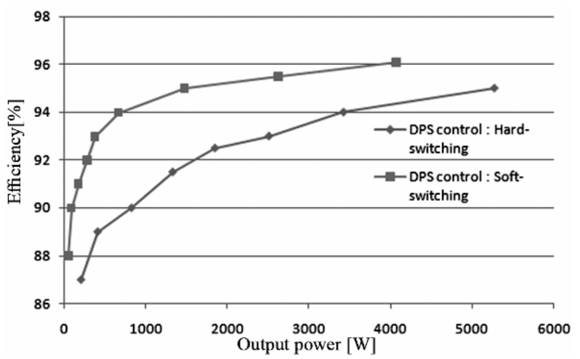

Fig. 15 –Efficiency comparisons DPS control : hard-switching *versus* soft-switching.

not similar to the ideal waveforms as shown in Fig. 5. In order to improve the overall efficiency of converter with dual phase shift control, a series resonant elements are connected at the primary side.

4.1 EFFICIENCY COMPARISONS

In this paper, mainly the efficiency analysis of SiC MOSFET based DAB with EPS and DPS controls under hard-switching and soft-switching conditions. The curves in Fig. 13 show the efficiency of DAB converter under hard-switching by means of varying the phase-shift angles. The efficiency curves shown in Fig. 13 are for different input voltages and output power as well. The efficiency improvement at 72° is about 95 % and 96 % efficiency achieved at 35° phase-shift angle. In addition to that, the efficiency comparisons also illustrated in Fig. 14 while DAB converter with additional resonant network. The efficiencies of about 96.5 % and 95.2 % were achieved at hard-switching condition. Similarly, performance analysis of SiC MOSFET based DAB with another control DPS was

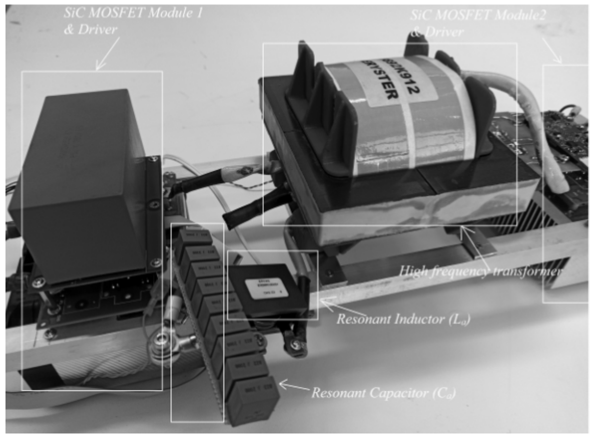

Fig. 16 – Photograph of SiC MOSFET DAB converter laboratory setup.

also performed under hard-switching and soft-switching conditions. Figure 15 shows the efficiency curves of DPS control. The maximum efficiency obtained for hard-switching condition is about 95.5 % at maximum output power 8 kW. The efficiency has been improved in DPS control with series resonant network at 8 kW is 96.5 %. By this performance analysis, EPS controlled DAB converter has improved efficiencies by varying the phase-shift angles and also impact of series resonant network. The efficiency of DPS control is also improved than the EPS. However, the DAB converter with series resonant network is much more effective than the hard-switching operation.

Similarly, performance analysis of SiC MOSFET based DAB with another control DPS was also performed under hard-switching and soft-switching conditions. Figure 15 shows the efficiency curves of DPS control.

The maximum efficiency obtained for hard-switching condition is about 95.5 % at maximum output power 8 kW. The efficiency has been improved in DPS control with series resonant network at 8 kW is 96.5 %. By this performance analysis, EPS controlled DAB converter has improved efficiencies by varying the phase-shift angles and also impact of series resonant network. The efficiency of DPS control is also improved than the EPS. However, the DAB converter with series resonant network is much more effective than the hard-switching operation. Figure 16 shows the photograph of laboratory setup of SiC MOSFET DAB converter used for the experimental analysis.

5. **CONCLUSIONS**

This article presented a SiC MOSFET based dual active bridge dc-dc converter suitable for electromobility applications such as charging the vehicle battery. The DAB converter operation principles and their analysis have been described. The SiC MOSFET based DAB converter performance has been verified by single phase shift, extended phase shift and dual phase shift control by using the same parameters. Initially, the hard-switching version of DAB converter is evaluated. In order to increase the overall gain, efficiency, minimized current stresses, the soft-switched DAB also measured. Based on the obtained results, the DAB converter with extended phase shifts at primary side is achieved 94.5 % and 96 % efficiency for soft-switched, both the case studies measured under 100 kHz switching frequency and efficiency operated at 8 kW output power. And also it is observed from the obtained results, the flow of back energy to the input side is minimized. Another dual phase shift control used on DAB converter is also verified. As from the efficiency analysis hard-switching version is 95.5 % and soft-switched is 96.5 % efficiency. Based on the obtained results, the selection of reliable and high efficient candidate like SiC MOSFET based dc-dc converter for electro-mobility applications is possible.

ACKNOWLEDGMENT

This research was supported by EU Regional and Urban Development – Operational Programme Smart Growth, Poland, project title 'Energy transfer system for electric vehicles integrated with lighting infrastructure', No. POIR.04.01.02-00-0052/16.

Received on November 21, 2018

REFERENCES

1. H. Krishnaswami, N. Mohan, *Three-Port Series-Resonant dc–dc Converter to Interface Renewable Energy Sources With Bidirectional Load and Energy Storage Ports*, IEEE Transactions on Power Electronics, **24**, *10*, pp. 2289–2297 (2009).
2. D. Christen, F. Jauch, J. Biel, *Ultra-fast charging station for electric vehicles with integrated split grid storage,* 2015 17th European Conference on Power Electronics and Applications (EPE'15 ECCE-Europe), Geneva, pp. 1–11 (2015).
3. G. E. Sfakianakis, J. Everts, E. A. Lomonova, *Overview of the requirements and implementations of bidirectional isolated AC-dc converters for automotive battery charging applications*,2015 Tenth International Conference on Ecological Vehicles and Renewable Energies (EVER), Monte Carlo, pp. 1–12 (2015).
4. A. Chakraborty, P.K. Sadhu, A. Chakrabarti, A. Basak, N. Pal, *Asymmetrical duty cycle phase-shifted dual output induction cooker***,** Rev. Roum. Sci. Techn. – Électrotechn. et Énerg., **63**, *1*, pp. 65–70 (2018).
5. N. M. L. Tan, T. Abe, H. Akagi, *Design and Performance of a Bidirectional Isolated dc–dc Converter for a Battery Energy Storage System*, IEEE Transactions on Power Electronics, **27**, *3*, pp.1237–1248 (2012).
6. K. Takagi, H. Fujita, *Dynamic Control and Performance of a Dual-Active-Bridge dc–dc Converter*, IEEE Transactions on Power Electronics, **33**, *9*, pp. 7858–7866 (2018).
7. K. Takagi, H. Fujita, *Dynamic control and performance of an isolated dual-active-bridge dc–dc converter,* 2015 9th International Conference on Power Electronics and ECCE Asia (ICPE-ECCE Asia), Seoul, pp. 1521–1527 (2015).
8. S. Inoue, H. Akagi, *A Bidirectional dc–dc Converter for an Energy Storage System With Galvanic Isolation*, IEEE Transactions on Power Electronics, **22**, *6*, pp. 2299–2306 (2007).
9. V.V.S.K. Bhajana, P. Drabek, M. Jara, *Design and analysis of a full bridge LLC dc-dc converter for auxiliary power supplies in traction*, Sādhanā, **43,** *6* (2018)
10. V.V.S.K. Bhajana, P. Drabek, M. Jara, *Performance evaluation of LLC resonant full bridge dc-dc converter for auxiliary systems in traction,* Rev. Roum. Sci. Techn. – Électrotechn. et Énerg., **60**, *1*, pp. 79–88 (2015).
11.. J. Everts, F. Krismer, J. Van den Keybus, J. Driesen, J. W. Kolar, *Optimal ZVS Modulation of Single-Phase Single-Stage Bidirectional DAB AC–dc Converters*, IEEE Transactions on Power Electronics, **29**, *8*, pp. 3954–3970 (2014).
12. S. Inoue, H. Akagi, *A Bidirectional Isolated dc-dc Converter as a Core Circuit of the Next-Generation Medium-Voltage Power Conversion System*, IEEE Transactions on Power Electronics, **22**, *2*, pp. 535–542 (2007).
13. S. Luo, F. Wu, *Hybrid Modulation Strategy for IGBT-Based Isolated Dual-Active-Bridge dc–dc Converter*, *IEEE Journal of Emerging and Selected Topics in Power Electronics*, **6**, *3*, pp. 1336–1344 (2018).
14. X. Liu ; Z. Q. Zhu, D.A. Stone, M.P. Foster ,W.Q. Chu, I. Urquhart, J. Greenough, *Novel Dual-Phase-Shift Control With Bidirectional Inner Phase Shifts for a Dual-Active-Bridge Converter Having Low Surge Current and Stable Power Control*, IEEE Transactions on Power Electronics, **32**, *5*, pp. 4095–4106 (2017).
15. T. Jiang, J. Zhang, X. Wu, K. Sheng, Y. Wang, *A Bidirectional LLC Resonant Converter With Automatic Forward and Backward Mode Transition*, IEEE Transactions on Power Electronics, **30**, *2*, pp. 757–770 (2015).
16. U. Kundu, B. Pant, S. Sikder, A. Kumar, P. Sensarma, *Frequency Domain Analysis and Optimal Design of Isolated Bidirectional Series Resonant Converter*, IEEE Transactions on Industry Applications, **54**, *1*, pp. 356–366 (2018).
17. M. Yaqoob, K. H. Loo, Y. M. Lai, *Extension of Soft-Switching Region of Dual-Active-Bridge Converter by a Tunable Resonant Tank*, IEEE Transactions on Power Electronics, **32**, *12*, pp. 9093–9104 (2017).
18. J. Dodge, *SiC JFET Cascode Enables Higher Voltage Operation in a Phase Shift Full Bridge dc-dc Converter*, PCIM Europe 2016; International Exhibition and Conference for Power Electronics, Intelligent Motion, Renewable Energy and Energy Management, Nuremberg, Germany, pp. 1–8 (2016).